Drug Design, Development and Therapy

Dovepress
open access to scientific and medical research

Open Access Full Text Article

ORIGINAL RESEARCH

Enhancement of Cancer Chemotherapeutic Efficacy via Bone-Targeted Drug Delivery Carrier in Bone Metastases

Xinghe Xue[1–4]
Jiachen Yu[1–4]
Fengfeng Lu[1–4]
Hongyi Jiang[1–4]
Xiangyang Wang[1–3]

[1]Department of Orthopaedic, The Second Affiliated Hospital and Yuying Children's Hospital of Wenzhou Medical University, Wenzhou, 325027, Zhejiang, People's Republic of China; [2]The Second School of Medicine, Wenzhou Medical University, Wenzhou, 325027, Zhejiang, People's Republic of China; [3]Key Laboratory of Orthopaedics of Zhejiang Province, Wenzhou, 325027, Zhejiang, People's Republic of China; [4]Wenzhou Institute, University of Chinese Academy of Sciences, Wenzhou, 325011, Zhejiang, People's Republic of China

Purpose: Bone metastases are common in malignant tumors, especially for the advanced cancers. Chemotherapy is an important treatment in clinic, but the application is limited due to the severe adverse reactions. We try to design bone-targeted drug delivery systems (DDS) for the delivery of chemotherapeutic drugs in bone metastatic carcinoma.

Material and Methods: We added alendronate (Aln) to metal organic framework (MOF) to synthesize a new bone-targeted DDS named Aln-MOF. Doxorubicin (DOX) as a classic anti-cancer drug was encapsulated. The material characterization, drug release and bone affinity were detected. In vitro experiment, the cell toxicity was detected by cck-8 test and cellular uptake were detected by laser scanning confocal microscope and flow cytometry. In vivo experiment, the pharmacokinetics of DDS in the blood was analyzed by fluorescence spectrophotometer and the biodistribution was detected by a multi-mode optical in vivo imaging system. The anti-tumor effects of MOF_{DOX} and Aln-MOF_{DOX} were evaluated by monitoring the tumor volume and weight during the animal experiment. In addition, the toxicity of DDS to different organs was determined by HE staining.

Results: Aln-MOF showed good stability, no cytotoxicity and better bone affinity than MOF. Both MOF_{DOX} and Aln-MOF_{DOX} could release DOX, and the release rate at pH = 5.5 was faster than the rate at pH = 7.4. The cellular uptake of Aln-MOF and MOF showed no difference. Aln-MOF had a long retention time in blood, which is beneficial for the enrichment of Aln-MOF in tumor sites. Aln-MOF mainly concentrated at bone metastases in mice. MOF_{DOX} and Aln-MOF_{DOX} could effectively delay tumor progression, and the effect of Aln-MOFDOX was more obvious ($P < 0.05$).

Conclusion: Our study confirmed that Aln-MOF has good stability, bone targeting and biosafety. Aln-MOF_{DOX} could release DOX and effectively kill tumor cells of bone metastases. Aln-MOF_{DOX} has a promising prospect in the treatment of bone metastasis.

Keywords: tumor, metal organic framework, alendronate, doxorubicin

Introduction

Bone metastases, which are common in malignant tumors, will cause physical and psychological damage to patients and seriously affect their normal life. Bone metastases mainly occur in advanced stage of tumors such as lung cancer, breast cancer and prostate cancer. The metastatic rate is 40–85% and the metastatic rate of prostate cancer is the highest which is up to 85%.[1,2] In addition to the above solid tumors, bone metastases can occur in 95% of multiple myeloma, which is a malignant plasma cell disease.[3]

Correspondence: Xiangyang Wang
Department of Orthopaedic, The Second Affiliated Hospital and Yuying Children's Hospital of Wenzhou Medical University, Wenzhou, 325027, Zhejiang, People's Republic of China
Tel\Fax +86-577-85676010
Email xiangyangwang@wmu.edu.cn

Received: 12 August 2021
Accepted: 14 October 2021
Published: 28 October 2021

The pathogenesis of bone metastases is still unclear. The tumor cells of primary malignant tumors (lung cancer, breast cancer, prostate cancer, etc.) migrate from their primary lesion to the circulatory system, mainly blood circulation. The tumor cells will metastasize to bone tissue and form bone metastases by the effect of different bone chemokines, such as connective tissue growth factor (CTGF), osteopontin (OPN) and IL-11 and so on. What's more, the surface molecules of bone endovascular skin also play an important role in the process of bone metastases formation.[4–6] The tumor cells often enter dormant state when they concentrate at bone tissue which can last years or even decades. Once the tumor cells are activated, they will rapidly proliferate and destroy bone tissue, causing a series of clinical symptoms. Lytic bone metastasis, which is the most serious type, will lead to skeletal related events (SREs), such as neoplastic pain, pathological fracture, tumor-derived hypercalcemia and spinal cord nerve compression.[7–9] The mechanism of dormancy and activation is still unclear.

Chemotherapy is an important means to treat primary tumors and bone metastases, such as doxorubicin (DOX). As systemic application of chemotherapy drugs, it will cause severe adverse reactions for the lack of tumor targeting ability.[5,10,11] In order to reduce the adverse reactions of chemotherapy drugs, some special materials can be selected as drug delivery systems (DDS). We can modify bone-targeting molecules to these DDS to provide bone-targeting properties. As a result, these new DDS are chosen to serve as drug delivery carriers to deliver chemotherapy drugs to bone metastases. At present, bisphosphonates especially alendronate (Aln) are the most widely used for bone targeting. Aln has a high affinity to hydroxyapatite in bone tissue. Aln can modify a variety of materials to provide bone targeting property, which has been confirmed in many studies.[12,13]

These DDS must have good biocompatibility and drug loading capacity. According to the structure and composition of DDS, they can be divided into organic DDS and inorganic DDS. The organic DDS have good biocompatibility and biodegradability,[14] while inorganic DDS are easily controllable in size, shape and functionalize.[15,16] Metal organic framework (MOF) is formed by the polymerization of iron, zinc, calcium and other metals through the bonding of imidazoles, amines and phosphonates. Because of the special construction combining both inorganic matters and organic matters, MOF has advantages of both organic and inorganic DDS. MOF has high porosity, high surface area, good thermal and chemical stability, which lead to excellent drug loading capacity and drug leakage resistance.[17–22] Recently, Tan et al synthesized a new multifunctional MOF-based nanohybrids which combined MOF with thermosensitive hydrogels. DOX and celecoxib were both loaded to treat localized oral cancer and the therapy efficacy and cell internalization were evaluated. This new nanocomposite showed unique biological abilities in terms of pH-responsiveness, antitumor efficacy and biocompatibility.[23] MOF seems to be a promising DDS for cancer treatment.

In this study, we constructed a mouse model of breast cancer bone metastases. We modified MOF with Aln and compound a new bone-targeting DDS (Aln-MOF) to deliver chemotherapy drug to bone tissue. Our study consisted four parts: synthesis of MOF and Aln-MOF, material characterization testing, in vitro cell experiments and in vivo animal experiments. The purpose of our study was to confirm that Aln-MOF had good biological safety, stability and bone targeting. When DOX was encapsulated in Aln-MOF, it could effectively treat bone metastases and reduce the cytotoxicity of DOX to other normal organs.

Materials and Methods

Materials

Zinc nitrate hexahydrate, dimethylimidazole, methyl alcohol and DOX were obtained from baichuan Biotech company (China). Cy5 and Rhob were obtained from Liuhe Biotech company (China). Dulbecco's Modified Eagle Medium (DMEM) was purchased from Huantai Inc. (Gibco, Grand Island, USA). 4′,6-Diamidino-2-phenylindole (DAPI) (Sigma-Aldrich, St Louis, USA) and fluoromount aqueous mounting medium (Sigma-Aldrich, St. Louis, USA) were obtained from Xinri Biotech company and used according to the manufacturer's instructions. Fetal bovine serum (FBS, ExCell Bio, Shanghai, China) was purchased from Huihong Biotech company. Other reagents were purchased from Sangon and used as received.

Synthesis of MOF, Aln-MOF, MOF_{DOX} and Aln-MOF_{DOX}

Zeolitic imidazole framework (ZIF) is one type of MOF. ZIF-8 is a kind of topological nanoparticle formed by self-assembly of transition metal atoms with organic imidazole and its derivatives, which has good drug loading capacity

and biocompatibility. We chose ZIF-8 as our delivery system.

We synthesize MOF according to previously reported studies with a little modification.[24] Six hundred milligram zinc nitrate hexahydrate ($Zn(NO_3)$ $2{\cdot}6H_2O$) and 1.3g dimethylimidazole were dissolved in two glass bottles containing 10mL methanol in each one. The mixture of two solutions was placed on a magnetic agitator and stirred for 30 minutes (37°C, 600 $r{\cdot}min^{-1}$). Then we placed the stirred mixture in a centrifuge for 10 minutes (10,000 $r{\cdot}min^{-1}$) and removed the supernatant to get the centrifuge product. After repeated washing, the reactants were dried overnight in a vacuum lyophilizer to remove the solvent and stored at room temperature for further experiments.

30.5mm (8.2g) Aln was dissolved in 50mL methanol. We combined 2mL Aln solution (1.22mM) with 100mg prepared MOF and placed on a magnetic agitator for 48 hours (37°C, 600 $r{\cdot}min^{-1}$). The rest procedures were as same as the synthesis of MOF and we get Aln-MOF finally.

As the effective anti-tumor ability of DOX, we chose DOX as our chemotherapy drug. We encapsulated DOX in our prepared MOF and Aln-MOF. 12.5mM (6.8g) DOX was dissolved in 50mL methanol solution to prepare DOX solution for later use. We added 100mg prepared MOF or Aln-MOF to 2mL DOX solution (0.5mM DOX) and place the mixed solution on a magnetic stirrer for 48 hours (37°C, 600 $r{\cdot}min^{-1}$). Then, the procedures of centrifugation, washing and freeze-drying were done as we mentioned above. Finally, we got MOF_{DOX} and Aln-MOF_{DOX} which encapsulated DOX.

Morphological Detection

Transmission Electron Microscope (TEM) was used to take pictures of Aln-MOF and MOF to observe the morphology of the nanoparticles. X-ray Diffraction (XRD) at 30 kV and 10 mA was used to do the phase analysis, including Aln-MOF, MOF and Aln. In addition, the chemical structures were analyzed by a Fourier transform infrared spectrometer (FTIR) with a wavenumber range of 500–4000 cm^{-1}. The surface composition and elemental valence were identified by X-ray photoelectron spectroscope (XPS).

The prepared MOF 50mg and Aln-MOF 50mg were respectively dissolved in 10mL PBS with 10% FBS to prepare a solution of 5mg/mL. The prepared solution was placed in Zetasizer Nano ZEN3600 dynamic light scattering tester to detect the nanoparticle diameter of MOF and Aln-MOF. Then, at different time points (2, 4, 8, 24, 48, 72h), the average diameter of MOF and Aln-MOF was detected to analyze the stability.

Detection of Drug Release Kinetics

The prepared MOF_{DOX} 50mg and Aln-MOF_{DOX} 50mg were respectively dissolved in 10mL distilled water to prepare a solution of 5mg/mL. UV spectrophotometer was used to detect the concentration of DOX in the solution. The wavelength of 480 nm was selected and blank MOF particles were used as the basic correction. Then the drug load of the two particles was calculated by the formula below: $LC = W_0/W_1$, W_0 was the amount of DOX in the particle, W_1 was the number of MOF or Aln-MOF particles.

The particles would meet two different pH values when entering into the body, the environment of blood (pH = 7.4) and intracellular lysosomal enzymes (pH = 5.5). Thirty-milliliter PBS with different pH values was added into the dialysis tube and the pH values were adjusted to 5.5 and 7.4, respectively. Twenty-milligram MOF_{DOX} and Aln-MOF_{DOX} was added into the dialysis tube, respectively. After stirring on a magnetic agitator (37°C, 100 $r{\cdot}min^{-1}$), 1mL solution, containing 500μL MOF_{DOX} or Aln-MOF_{DOX} and 500μL PBS with different pH, was detected by microplate reader to calculate the concentration of DOX at different time point (0.5, 1, 2, 4, 6, 8, 12, 24, 48 h).

Bone Affinity Test

The bone affinity of the prepared Aln-MOF and MOF was detected by ultraviolet spectrophotometer. Three hundred microgram Aln-MOF and MOF were added into an EP tube containing 500μL distilled water (c_0=0.6μg/μL). The tibia of the mice was taken and added into the above solution. After the mixture was placed on a constant temperature shaker for 24 hours at room temperature for 24 hours, the particle concentration c_1 of the remaining liquid was detected by ultraviolet spectrophotometry. The bone affinity was calculated according to the formula:

$$BDA(BondBindingaffinity)\ (\%)=(c_0-c_1/c_0)x100\%.$$

Mouse Breast Cancer 4T1 Cell Culture

The Mouse breast cancer 4T1 cells were purchased from American type culture collection (ATCC). The 4T1 cells were inoculated in RRMI-1640 medium containing 10% FBS+1% dual antibodies, and then cultured in carbon

dioxide incubator (37 °C, 5%CO_2). The medium in the culture dish should be changed every other day, and the 4T1 cell was passaged every 3 days. We chose the second or third generation as our experimental subjects. All the experimental cells are in logarithmic growth.

Cck-8 Test

We need to detect the cytotoxicity of three groups of nanoparticles, namely Aln-MOF, MOF_{DOX} and Aln-MOF_{DOX}. According to the concentration of DOX drug, it was divided into 0.25, 0.5, 1.0, 2.0, 4.0μg/mL groups from low to high (the drug loading of particle DOX was 0.65μg/mg). Cck-8 test was used to detect the cytotoxicity.

Laser Scanning Confocal Microscopy

DAPI, Alexa Fluo 488 and RhoB were used to label the cell nucleus, cytoskeleton and nanoparticles of the 4T1 cells, respectively. Then, laser scanning confocal microscopy was used for imaging analysis. Finally, the fluorescence intensities of MOF and Aln-MOF were compared.

Flow Cytometric Analysis

RhoB was used to stain MOF and Aln-MOF particles. Then, flow cytometry was used to quantitatively analyze the cells uptaking RhoB-stained MOF and Aln-MOF. The difference of the cell number and fluorescence intensity of RhoB positive cells were counted to calculate the uptake of MOF and Aln-MOF by the 4T1 cells.

Animal Model

We selected Balb/c mice as our experimental animal, which were authorized by the Animal Protection and Utilization Committee of University of Chinese Academy of Sciences and provided by Vital River Laboratories (Beijing, China). All the parts involving animal experiment ethics in our study have been reported to the Animal Ethics Committee of University of Chinese Academy of Sciences for approval (WIUCAS21071205). All the animal experimental procedures were consistent with the national standard "Laboratory Animal-Guideline for Ethical Review of Animal Welfare" (GB/T35892-2018) of China.

The 4T1 cells were allocated into a certain proportion (cell concentration =10^4/μL). 50μL of the cell solution was injected into the bilateral tibia of Balb/c mice to establish the animal model of bone metastasis.

Duration of MOF and Aln-MOF in Blood

We used MOF and Aln-MOF particles to encapsulate Cy5 fluorescent molecules in the same way as DOX was encapsulated. We dissolve MOF_{Cy5} and Aln-MoF_{Cy5} in distilled water (5mg/mL). Then we combine 360ul MOF_{Cy5} or Aln-MOF_{Cy5} solution and add 40μL 10X PBS to prepare isotonic liquid which was injected into mice through the caudal vein. At different time points (0.5, 1, 2, 4, 6, 8, 12, 24, 48h), 200μL orbital blood was collected and centrifuged at 3000 rpm for 5 minutes to obtain the serum for detection. The concentration of MOF_{Cy5} or Aln-MOF_{Cy5} in serum at different time points was detected by fluorescence spectrophotometer.

Distribution of MOF and Aln-MOF

We used a multi-mode optical in vivo imaging system to detect the distribution of MOF and Aln-MOF in mice. After establishing mice with bone metastases for 2 weeks, we injected 400μL isotonic solutions (360μL of MOF_{Cy5} or Aln-MOF_{Cy5} solution +40μL 10X PBS) into mice through the caudal vein. The distribution of MOF_{Cy5} or Aln-MOF_{Cy5} was detected by the multi-mode optical in vivo imaging system at different time points (0.5, 2, 6, 24h). At 24h, the mice were sacrificed and different organs were detected by the multi-mode optical in vivo imaging system.

The Therapeutic Effect of MOF_{DOX} and Aln-MOF_{DOX}

When the tumor volume of bone metastases reached at least 50mm^3, the anti-tumor therapeutic effects of MOF_{DOX} and Aln-MOF_{DOX} were tested in vivo. The experimental mice were divided into the following 5 groups: PBS group, Aln-MOF group, DOX group, MOF_{DOX} group and Aln-MOF_{DOX} group. Each group had 5 mice. The mice were treated by PBS, Aln-MOF, DOX, MOF_{DOX} and Aln-MOF_{DOX} through the caudal vein every 3 days for up to 4 times, respectively. The dose of DOX 5mg/kg in group DOX, MOF_{DOX} and Aln-MOF_{DOX}. Group PBS was treated with equal volume of PBS as blank control, and group Aln-MOF was treated with equal dose of Aln-MOF to group Aln-MOF_{DOX}. The mice were weighed on day 2, 4, 6, 8, 10, 12, 14, 16 and 18, and the tumor volume was calculated at the same time. The tumor volume was calculated by the following formula: $\text{tumorvolume} = \left(\text{lengthX}(\text{width})^2\right)/2$. The length and width of the tumor were measured at the bone metastases using vernier caliper.

On the 18th day, the mice were sacrificed and the bone metastatic tumor specimens were dissected and weighed. At the same time, tumor specimens of three typical mice were selected and photographed for recording. Sections and HE staining were performed on different tissues of the sacrificed mice, including heart, liver, spleen, lung, kidney and bone. Then different tissues were observed under a microscope for comparison.

Statistical Analyses

At least three independent tests were conducted, and the measured data were expressed as mean ± standard deviation (SD). Statistical analysis was performed by SPSS software, followed by Tukey's test. $P < 0.05$ was considered statistically significant.

Results

Material Characterization

The morphological appearance of ALN-MOF and MOF were observed under TEM (Figure 1A and B). The diameters of the prepared MOF and Aln-MOF were basically around 110 nm, while the Aln-MOF size was slightly larger (Figure 1C). We detected the size changes of two nanoparticles at different time points (2, 4, 8, 24, 48, 72h), and found that the diameters did not change significantly and the stability was good (Figure 1D). Although the aggregation of nanoparticles happened, the effective size would not bigger than cells of micron level. As a result, the particle aggregation could not block blood vessels in some organs with tiny blood vessel such as liver, brain and lung.

The FTIR spectra of Aln, MOF and Aln-MOF were analyzed (Figure 2A). In the FTIR spectra of Aln, the peak at 914, 1017, 1047 cm^{-1} corresponded to stretching vibration of P-O, P-C and P=O groups, respectively. The characteristic phosphate group peak was obtained at 1545 cm^{-1}, N-H stretching peaks were observed at 3482 cm^{-1}. For the spectral MOF, C=N stretching peaks was observed at 1596 cm^{-1}, the peak of 1046 cm^{-1} was attributed to C-N symmetric stretching, the most intense peaks at 1153 and 1114 cm^{-1} corresponded to C-N in-plane stretching, which also appeared

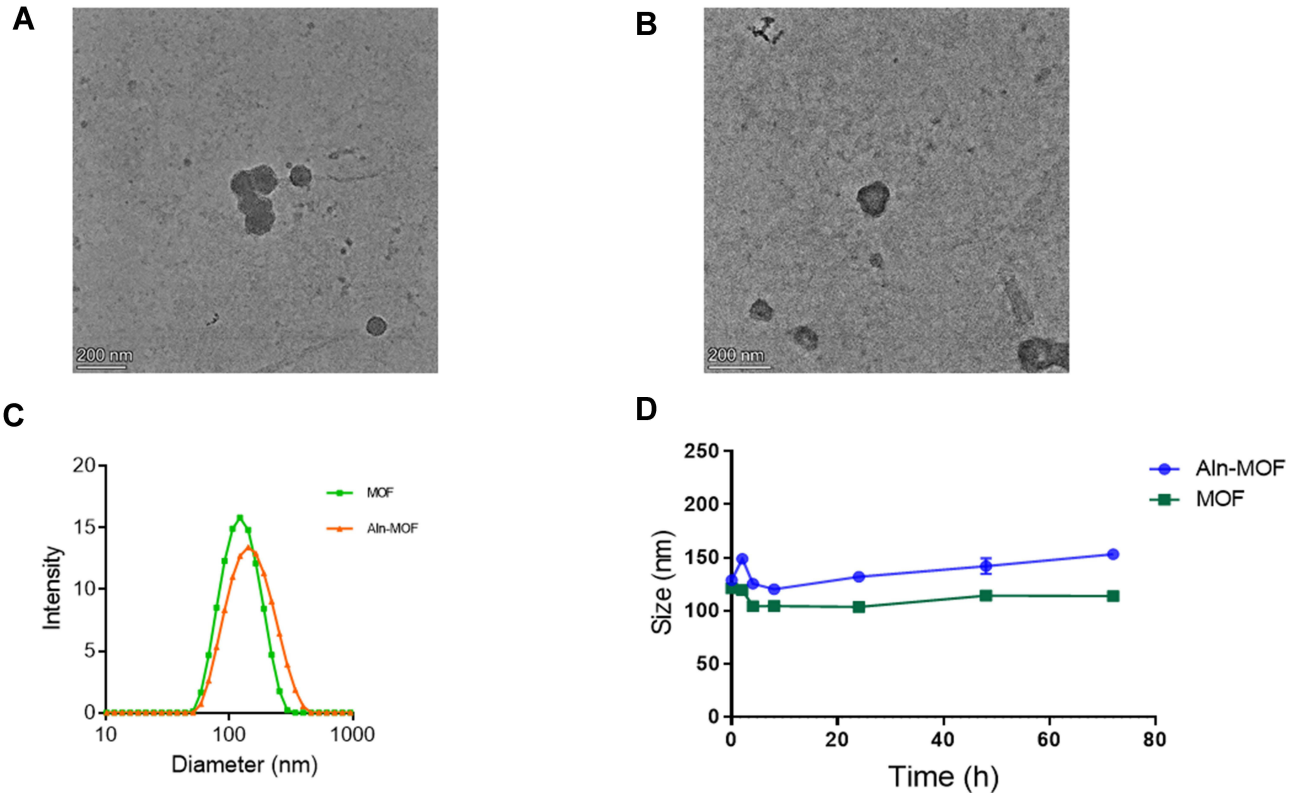

Figure 1 Transmission electron microscopy (TEM) and dynamic light scattering tests.
Notes: (**A**) The morphology of Aln-MOF under TEM. (**B**) The morphology of MOF under TEM. (**C**) The particle diameters of MOF and Aln-MOF were about 110 nm, while Aln-MOF was slightly larger. (**D**) The diameters of the two particles did not change significantly at different time points (0, 2, 4, 8, 24, 48 and 72h).
Abbreviation: TEM, transmission electron microscopy.

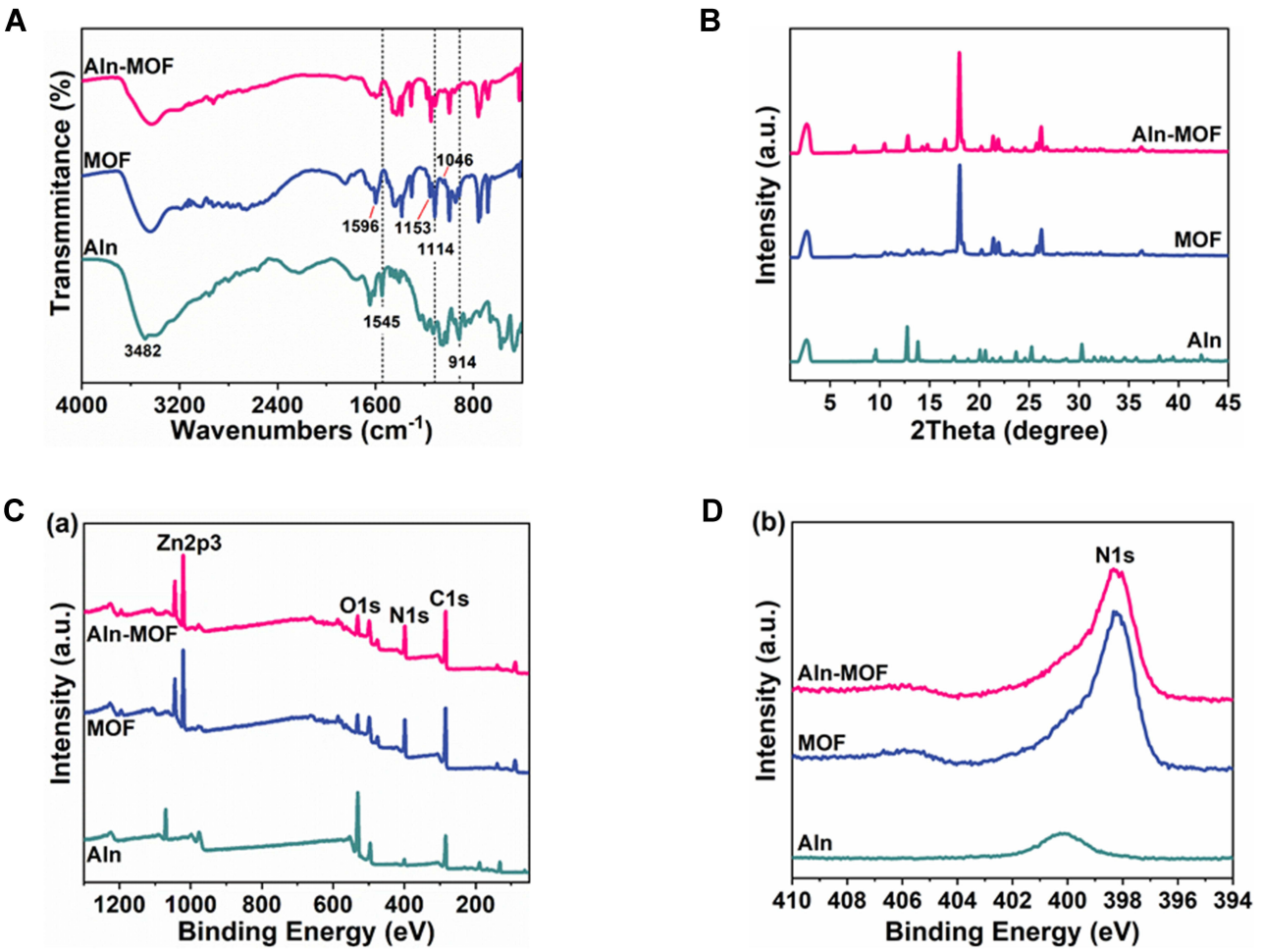

Figure 2 The analysis of FTIR, XRD and XPS.
Notes: (**A**) FTIR spectra of Aln, MOF and Aln-MOF. (**B**) XRD patterns of Aln, MOF and Aln-MOF. (**C** and **D**) XPS spectra of Aln, MOF and Aln-MOF. (**C**) (a) Survey spectra of XPS. (**D**) (b) N1s spectra of XPS.
Abbreviations: FTIR, Fourier transform infrared spectroscopy; XRD, x-ray diffraction; XPS, x-ray photoelectron spectroscopy.

in the spectrum of Aln-MOF, the peaks at 1302, 944, 756 and 680 cm^{-1} were from C-H bending in imidazole ring. The absence of characteristic phosphate peak of Aln at 1545 cm^{-1} could be considered as Aln molecules were encapsulated into MOF instead of attachment to MOF surface.

The XRD results indicated the highly crystalline formation of Aln and MOF. The XRD pattern of Aln-MOF sample was almost in agreement with MOF, and the intensity of Aln peaks was greatly reduced, suggesting that Aln molecules were efficiently encapsulated by the MOF cages, and the introduction of Aln did not cause loss of crystallinity (Figure 2B). The XPS of Aln-MOF showed a slight red shift in the N 1s binding energy, indicating that the coordination interaction between the Aln and MOF and the increased relative amount of N signal confirmed the presence of Aln in Aln-MOF (Figure 2C and D).

Drug Release Kinetics

According to the formula which mentioned above, the DOX loaded capacity of MOF and Aln-MOF particles was 0.65μg/mg. It showed that Both MOF and Aln-MOF particles could release DOX lasting for 12 hours. The release rate at pH = 5.5 was faster than that at pH = 7.4 (Figure 3). As a result, after entering bone metastatic cells from blood, Aln-MOF_{DOX} could quickly release DOX to the tumor cells due to pH changes. This pH-related characteristic was previously found in many other materials which further proved the reliability of our result.[25,26]

Bone Affinity

When pH = 7.4 (simulated blood), the concentration of Aln-MOF was significantly reduced compared with MOF and the bone affinity of Aln-MOF was higher than MOF ($P < 0.01$). Similarly, when pH = 5.5 (simulating

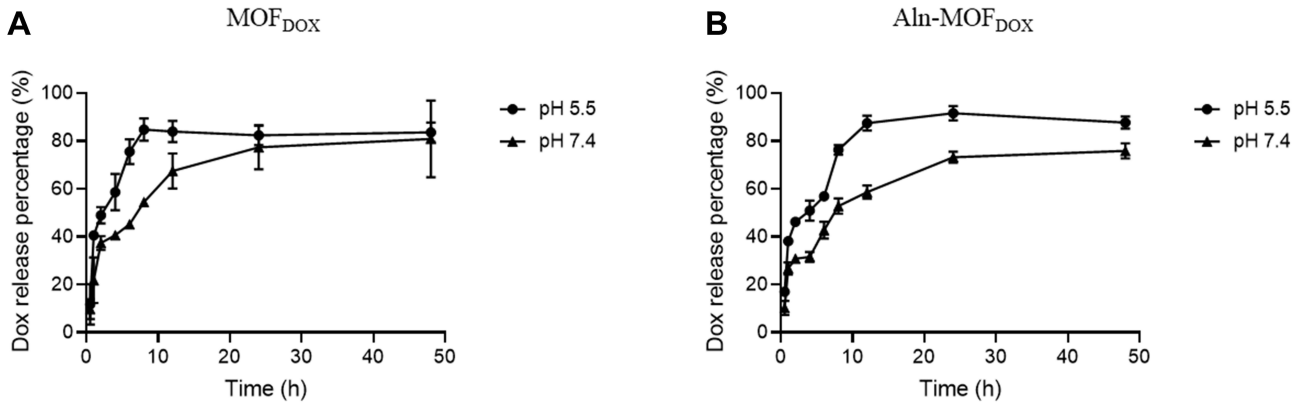

Figure 3 Detection of drug release in MOF and Aln-MOF at different pH.
Notes: (**A** and **B**) At pH = 7.4 (simulated blood) and pH = 5.5 (simulated intracellular lysosomal enzyme), both MOF$_{DOX}$ and Aln-MOF$_{DOX}$ could gradually release DOX to a peak within 12h. The release rate of DOX in Aln-MOF$_{DOX}$ at pH = 5.5 is faster than that at pH = 7.4.

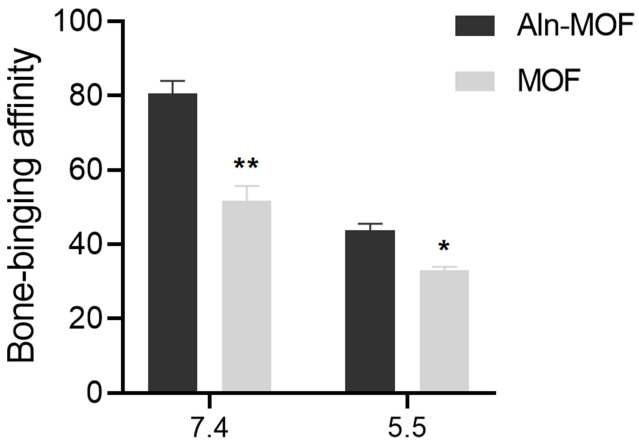

Figure 4 Bone-binging affinity test.
Notes: No matter pH = 7.4 or pH = 5.5, Aln-MOF showed better bone affinity than MOF. The formula for calculating bone affinity: $BBA(\%)=(c_0-c_1/c_0)x100\%$, where c_0 is the particle concentration of the original solution and c_1 is the particle concentration of the remaining solution after mixed with bone tissue for 24 hours. Significant differences between groups were indicated as $^{**}p < 0.01$, $^{*}p < 0.05$.
Abbreviation: BBA, bone-binging affinity.

intracellular lysosomal enzymes), the bone affinity of Aln-MOF was also higher than that of MOF ($P < 0.05$) (Figure 4). No matter pH = 7.4 or pH = 5.5, Aln-MOF could provide good bone targeting property compared with MOF.

Cytotoxicity

When the concentration of Aln-MOF increased, it had no cytotoxic effect on the 4T1 mouse cells which proved that Aln-MOF showed almost no cytotoxicity and reliable biological safety. After Aln-MOF and MOF were encapsulated with DOX, the cytotoxic effect of Aln-MOF$_{DOX}$ and MOF$_{DOX}$ on the 4T1 cells was obvious. The cytotoxic effect was enhanced by increasing the concentration (Figure 5).

Cellular Uptake

Confocal laser detection (Figure 6A and B) and flow cytometry (Figure 6C and D) were used to detect cellular uptake of Aln-MOF and MOF in the 4T1 cells. The cells could absorb Aln-MOF and MOF (Figure 6A), but it showed that the fluorescence intensities of RhoB stained Aln-MOF and MOF were similar (Figure 6B). The same result could be found in the positive cell rate and fluorescence intensity by flow cytometry (Figure 6D and E). The similar cellular uptake of Aln-MOF and MOF indicated that Aln did not influence MOF except providing bone targeting property.

Nanoparticles Distribution in vivo

Aln-MOF stayed in the blood for a longer time than MOF which was in favour of enrichment in bone metastases (Figure 7A). At 24 hours after injection, it could be seen that the concentration of Aln-MOF in the bone metastases was higher than MOF. Although MOF could enrich in the bone metastases, it would be eliminated quickly (Figure 7B). Mice were sacrificed at 24h after injection. It showed that Aln-MOF mainly concentrated at the bone metastases. However, MOF mainly concentrated in the liver, followed by bone metastases. The Aln-MOF concentration at the bone metastases was higher than MOF ($P < 0.05$) (Figure 8).

Anti-Tumor Effect

The tumor volumes of bone metastases at different time points were calculated, and we found that Aln-MOF had

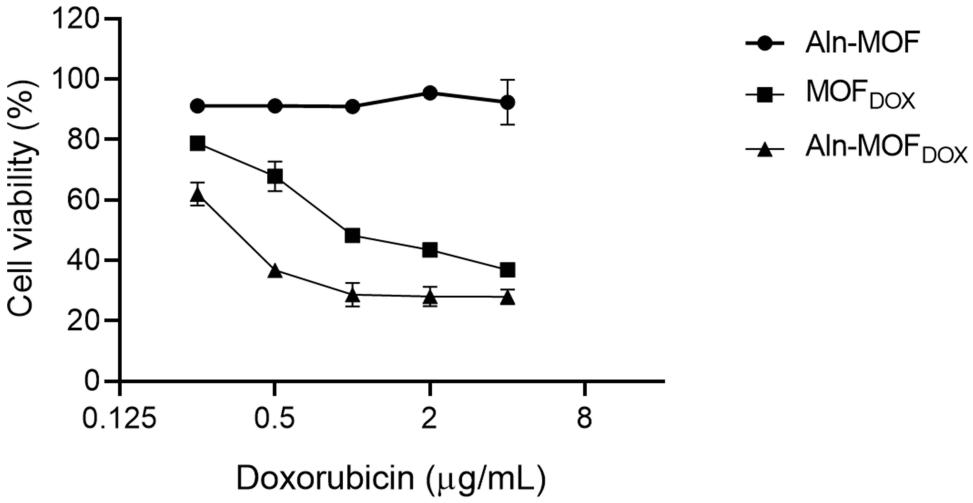

Figure 5 Cytotoxicity of the nanoparticles.
Notes: Aln-MOF had no toxicity to breast cancer 4T1 mouse cells and has good biosafety. After encapsulated with DOX, MOF and Aln-MOF could effectively kill the 4T1 cells.

no effect on the proliferation of bone metastases while MOFDOX and Aln-MOFDOX could significantly slow down the tumor growth compared with PBS (Figure 9A). But the effect was limited and the tumor volume initiated to increase after 12 days which are similar to previous study.[27] The drug withdrawal of Aln-MOF$_{DOX}$ would cause recurrence of the disease, indicating that Aln-MOF$_{DOX}$ had useful effect but might require long-term use. The treatment plan might not be enough, and the therapeutic effect could be maximized by optimizing the frequency of administration. The body weight at different time points had no significant difference among the 5 groups (Figure 9B). Generally, drugs with high toxicity would cause weight loss. This experiment proved that our Aln-MOF and Aln-MOF$_{DOX}$ were biological safe. Aln-MOF$_{DOX}$ could significantly reduce the weight of tumor tissues and slow down tumor growth, and the therapeutic effect of Aln-MOF$_{DOX}$ was more obvious compared with DOX ($P < 0.01$) and MOF$_{DOX}$ ($P < 0.05$) (Figure 9C). The photographs of three typical tumor specimens were recorded (Figure 9D).

HE staining was performed (Figure 10) and found that Aln-MOF and Aln-MOF$_{DOX}$ had no obvious toxicity to other organs except for bone metastases. However, in tumor tissues, compared with other groups, the nuclei of tumor cells in group Aln-MOF$_{DOX}$ reduced, which indirectly indicated that Aln-MOF$_{DOX}$ had a killing effect on tumor cells. It could be seen that the Aln-MOF$_{DOX}$ had a good bone targeting property and minimize adverse reactions to other normal organs.

Discussion

In this study, MOF nanoparticles were selected as our DDS to deliver chemotherapy drug DOX. In order to obtain bone targeting property, we modified MOF with Aln and synthesized a new bone targeted DDS named Aln-MOF. Our study mainly proved that Aln-MOF had good bone targeting and biological safety. After DOX was encapsulated in Aln-MOF, Aln-MOF$_{DOX}$ could effectively kill the tumor cells of bone metastases without affecting the normal cells in other tissues. Aln-MOF could accurately deliver DOX to bone metastases and reduce the adverse reactions rate caused by DOX. MOF had been applied in the field of biomedicine, but not been used in the treatment of bone metastases in the world.

Bone metastases often cause bone metabolism imbalance especially osteolysis which will lead to SREs. Osteoblasts and osteoclasts are two important cells in bone tissue. Osteoblasts provide positive promotion for the formation of bone tissue while osteoclasts do the opposite. In normal physiological state, in order to meet the different physiological needs of the host, the microenvironment of bone tissue cells is strictly regulated. Osteoblasts and osteoclasts are in a balanced state to maintain normal bone mass.[28–30] Once bone metastases occur, both osteoblast and osteoclast are activated, but the balance is closely related to the primary tumor.

In the previous studies, DDS such as nanoparticles have been used as carriers of chemotherapy drugs and widely used in the treatment of bone metastases.[31–34] Among them, liposome is the most widely used DDS,

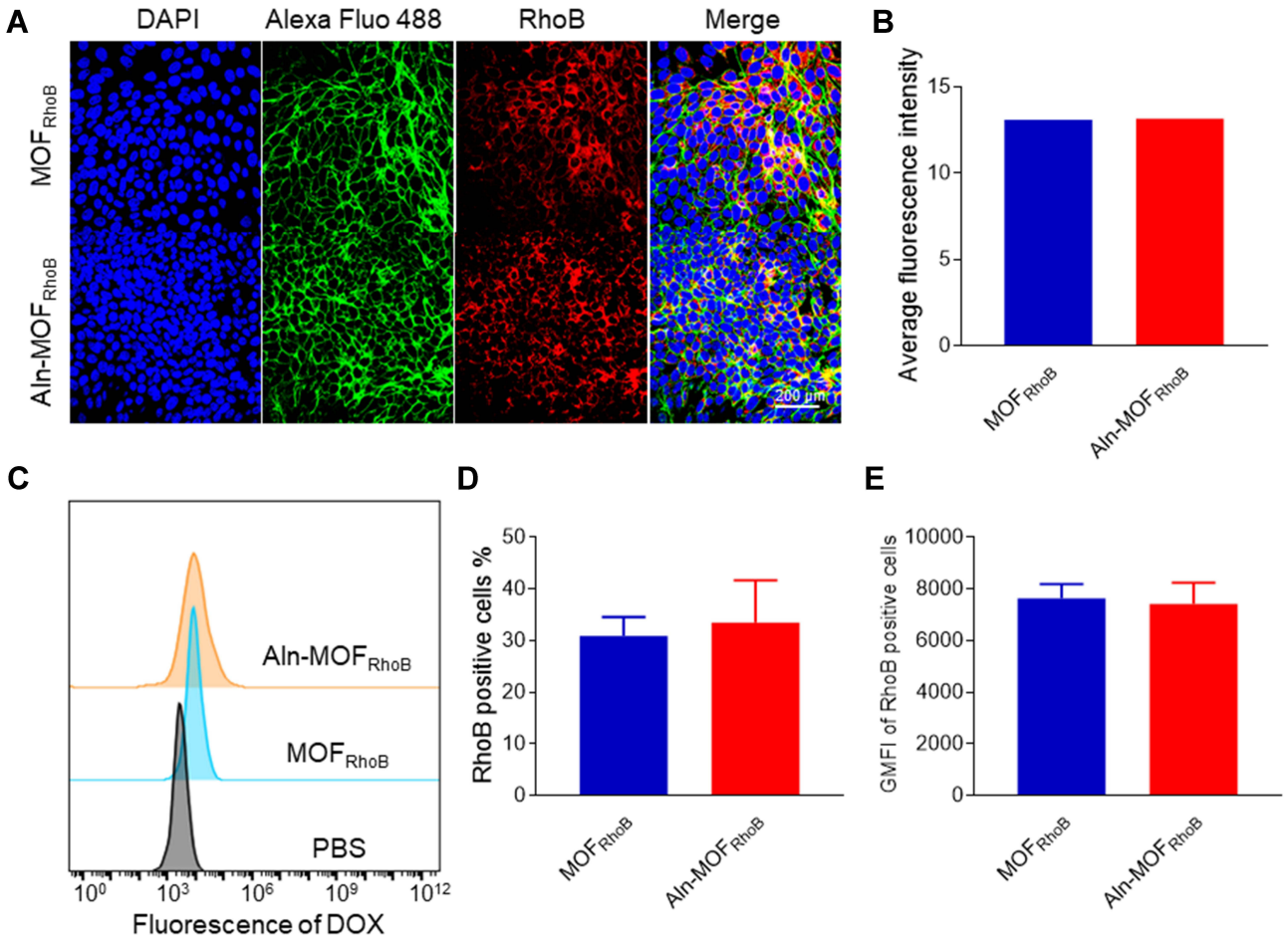

Figure 6 The cellular uptake of MOF and Aln-MOF by breast cancer 4T1 mouse cells were detected by laser confocal detection and flow cytometry.
Notes: (**A**) DAPI, Alexa Fluo 488 and RhoB were used to stain the cell nucleus, cytoskeleton and prepared nanoparticles. Finally, mixed images were synthesized, which showed that the cells could absorb Aln-MOF and MOF. (**B**) There was no significant difference between the amount of RhoB-stained Aln-MOF and MOF. (**C**) Flow analysis diagram. (**D**) There was no significant difference in the number of RhoB-stained Aln-MOF and MOF ($P > 0.05$). (**E**) There was no significant difference in the fluorescence intensity between RhoB-stained Aln-MOF and MOF ($P > 0.05$).

which is synthesized by lecithin and ceramide and belongs to organic DDS. Although organic DDS have good biocompatibility, the morphology and function controllability of organic DDS are poor compared with inorganic DDS. Inorganic DDS, such as SiO_2 particles, are easy to synthesize. They also can easily change their morphology and drug loading property according to the needs of treatment. For this reason, we chose MOF which combining inorganic and organic materials as our raw nanoparticles. Compared with traditional drug carriers such as whether organic or inorganic DDS, MOF inherited part advantages of both DDS.

No matter which DDS is to be used in vivo, the most important prerequisite is biocompatibility. Many materials, especially inorganic materials, will not be further used even if they have good drug loading and releasing property due to their biological toxicity. Our research group has demonstrated the biocompatibility and biosafety of Aln-MOF in both cells and mice through multiple experiments. In vitro, Aln-MOF was co-cultured with the 4T1 cells, and no cytotoxicity was observed. In vivo, Aln-MOF did not cause weight loss in mice and HE staining showed Aln-MOF would not damage other normal organs. It can be seen that the Aln-MOF prepared by us has good biocompatibility and biosafety which is the preconditions for further research.

Renal excretion is the main excretion route for highly polar metabolites or drugs. In addition, it is also one of the most important ways for removing the wandering external materials from body. The free materials in the blood quickly accumulate in the kidney within 1 hour after intravenous injection, and rapid excretion is performed within 4–8 hours.[35–37] In our study, MOF accumulated in the kidney and was excreted quickly within 2 hours while

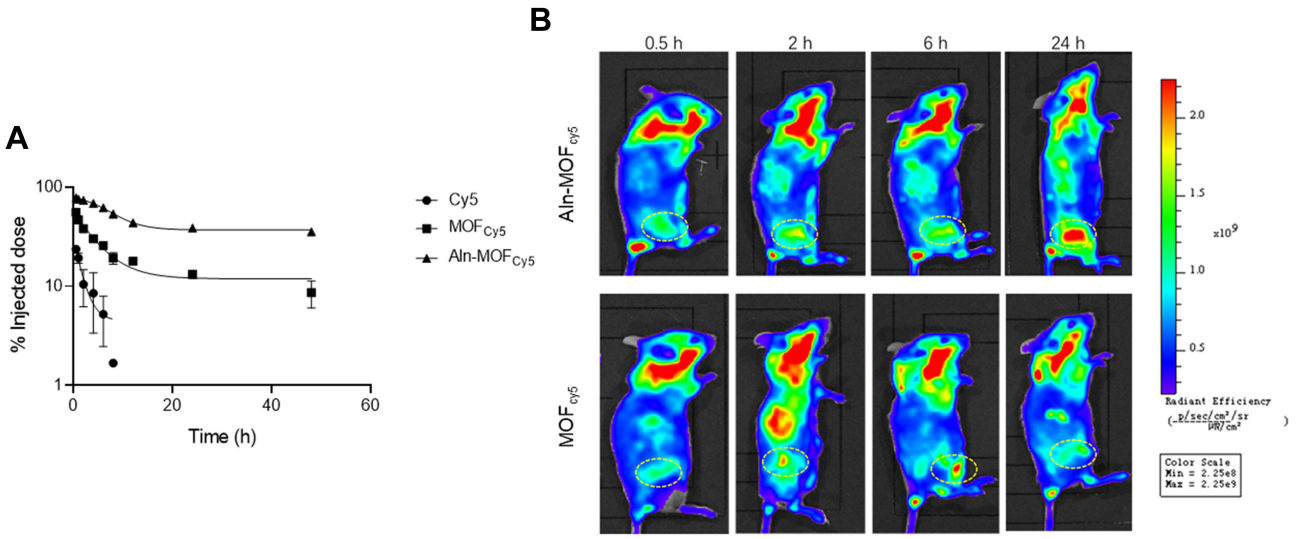

Figure 7 Distribution of MOF and Aln-MOF in mice.
Notes: (**A**) The blood duration of Aln-MOF was longer than MOF. The longer retention time of blood circulation was in favour of the nanoparticle enrichment at the tumor site. (**B**) The distribution of Aln-MOF and MOF were observed in mice using a multi-mode optical in vivo imaging system. MOF was rapidly eliminated, while Aln-MOF enriched at tumor site for a long time. At 24 hours, the amount of Aln-MOF at bone metastases site was larger than MOF.

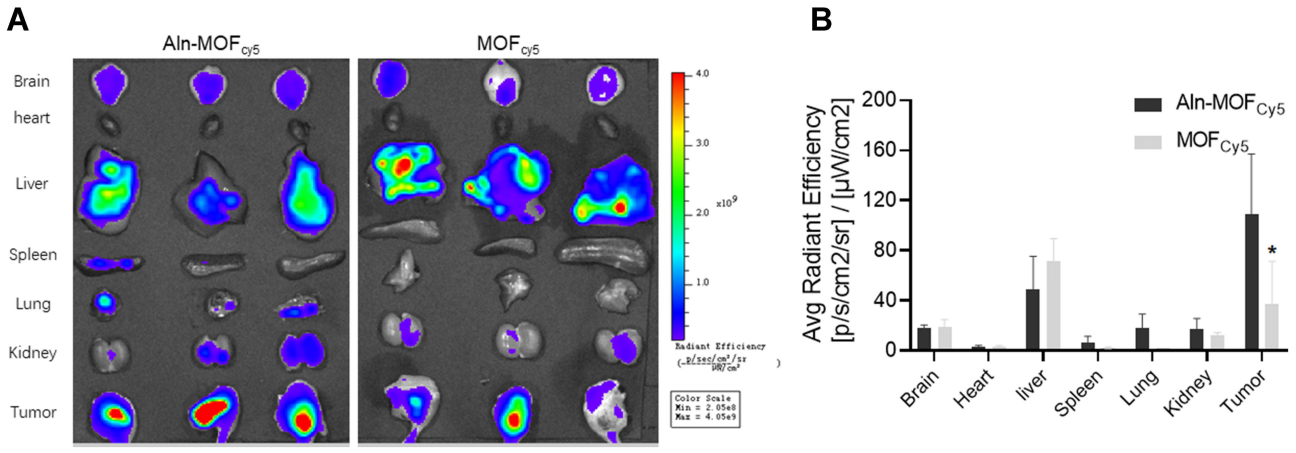

Figure 8 Distribution of MOF and Aln-MOF in different organs after sacrificing the mice at 24h after injection.
Notes: (**A**) Three mice's different organs were detected by a multi-mode optical in vivo imaging system. (**B**) Aln-MOF mostly concentrated at bone metastases site, indicating that Aln-MOF had good bone targeting, while MOF mainly concentrated in liver. It showed that the enrichment of Aln-MOF at bone metastases site was significantly higher than MOF. Significant difference between groups was indicated as *$p < 0.05$.

Aln-MOF accumulate in the kidney slowly and the renal excretion extended to 24 hours. This phenomenon might be related to the bone targeting of the material which was similar to previous studies.[27,36,37] Material accumulates in bone metastases, reducing the amounts of materials in blood circulation. As a result, the slower renal excretion of Aln-MOF also proved the bone targeting and long-term action of Aln-MOF.

At present, there are two main bone targeting mechanisms. One is to target bone-specific cells such as osteoclasts or osteoblasts in bone tissues, including the current major bone targeting drugs, such as RANKL monoclonal antibodies. The other is to target bone matrix such as hydroxyapatite, including bisphosphonates and so on.[38,39] It can be seen that bisphosphonate has a high affinity with hydroxyapatite. Aln is the third generation of bisphosphonates, and its safety and efficacy have been clinically proven. In this study, Aln-MOF nanoparticles were synthesized by using Aln as bone targeting molecule. Because of its good bone targeting property, Aln-MOF can be used as a drug carrier for the treatment of bone metastases. In our study, although Aln-MOF had good bone targeting, it still

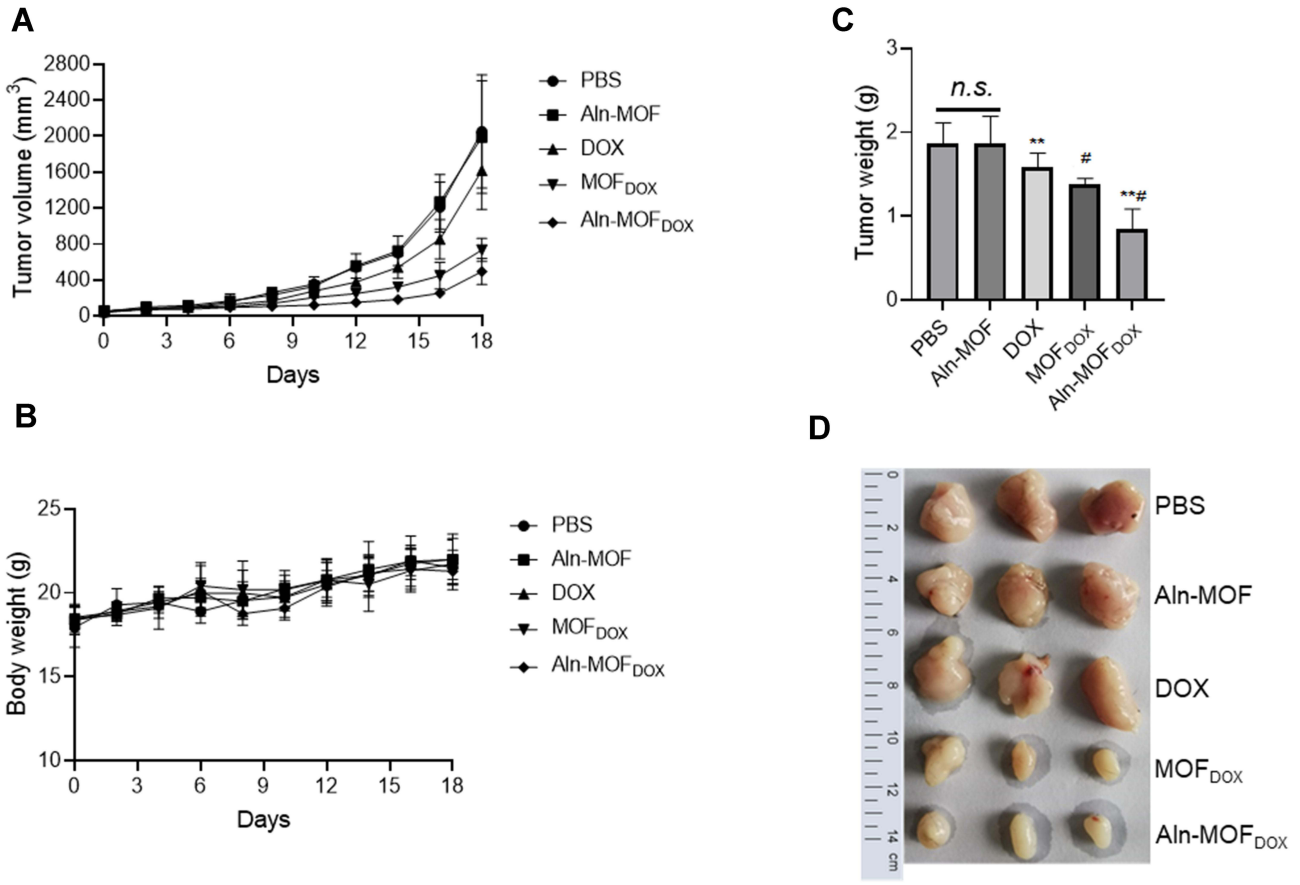

Figure 9 The changes of tumor volume and weight after different treatment were detected in animal experiments.
Notes: (**A**) The tumor volume of bone metastatic tumor was calculated on day 0, 2, 4, 6, 8, 10, 12, 14, 16 and 18, and it was found that Aln-MOF_{DOX} and MOF_{DOX} could slow down the growth of bone metastases compared with PBS. (**B**) No significant differences were found in the weight of mice on day 0, 2, 4, 6, 8, 10, 12, 14, 16 and 18, which proved that Aln-MOF and Aln-MOF_{DOX} were safe to body. (**C**) After the mice were sacrificed on day 18, the weight of tumor tissues in mice was calculated. Aln-MOF_{DOX} could significantly reduce the weight of tumor tissues compared with DOX ($p < 0.01$) and MOF_{DOX} ($p < 0.05$). (**D**) The photographs of three typical tumor specimens were recorded. Significant difference between groups was indicated as $^{**}p < 0.01$, $^{\#}p < 0.05$.

enriched in the liver which would affect the therapeutic effect to a certain extent. This phenomenon currently exists in many materials. At present, all targeted modification cannot avoid the removal effect of mononuclear phagocyte system (MPS) system in liver, and this is a difficult problem in the whole field of nano drug delivery. As a result, all the modifications of targeted therapy hope to improve the enrichment of the target region and improve the drug delivery effect as much as possible. The development of multiple therapeutic approaches is needed to solve liver clearance problem.

In addition, considering that most bone metastases are lytic bone metastases, Aln not only provides our nanoparticles bone targeting property but also has therapeutic effect on lytic bone destruction. Aln can play an important role in the following three aspects: 1. Aln directly acts on osteoclasts to change their morphology and promote apoptosis; 2. It binds to the bone matrix in the microenvironment of bone tissue and interferes with bone resorption. As a result, this will inhibit osteolysis. 3. It inhibits osteoblasts from releasing cytokines to repair damaged osteoclasts.[40–42] It can be seen that Aln-MOF can not only be used as a carrier to deliver chemotherapy drugs but also has therapeutic effect on osteolysis related to bone metastases.

Based on the good biocompatibility, bone targeting and drug release function of Aln-MOF, it laid the foundation for us to encapsulate DOX to treat bone metastases. The killing effect of DOX on tumor cells has been confirmed by previous clinical studies. DOX is applied in a variety of malignant tumors and has broad-spectrum anti-tumor effect. DOX inhibits macromolecular protein biosynthesis by interacting with tumor cell DNA, which further inhibits the synthesis of topoisomerase II and disrupts the DNA superhelix to interfere with transcriptional function. In addition, DOX can also produce free radicals and induce DNA and cell membrane damage.[43,44]

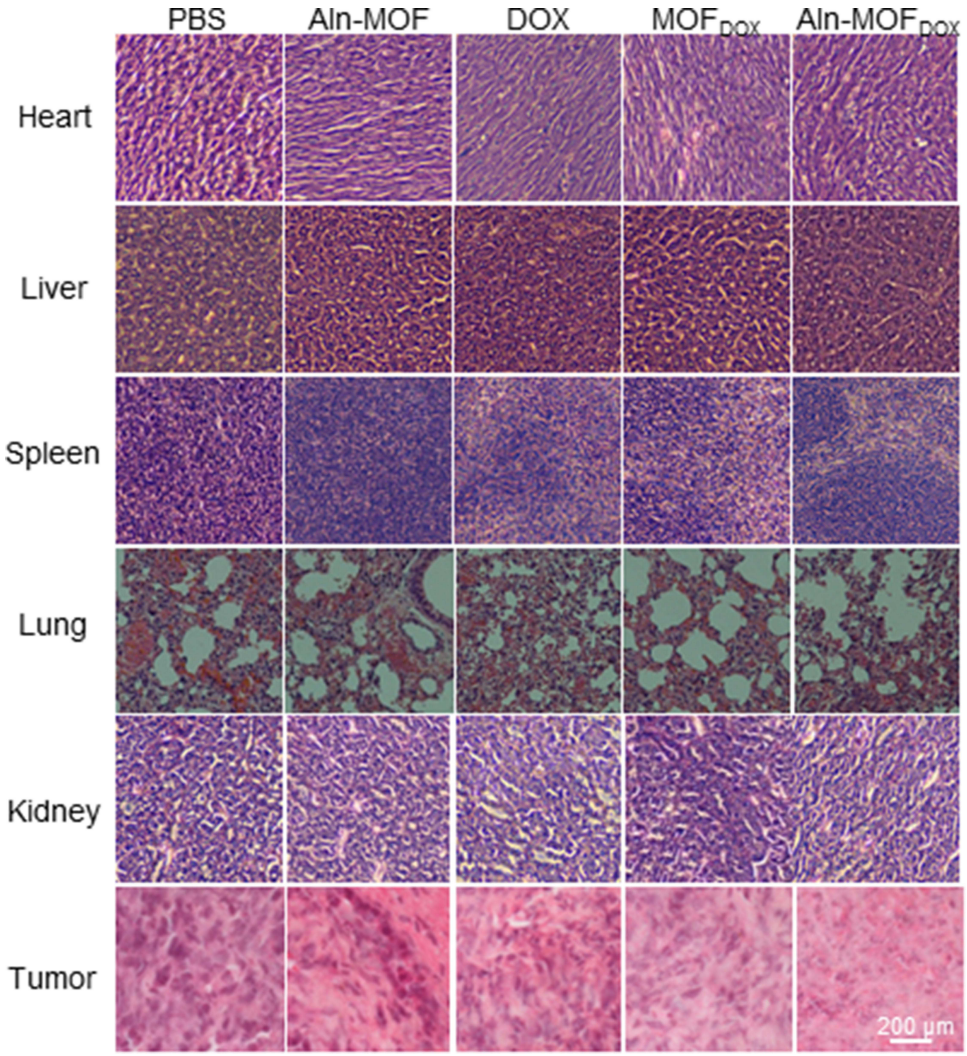

Figure 10 HE staining of different tissues containing heart, liver, spleen, lung, kidney and tumor (bone metastases) on day 18.

But our study still has some limitations. First, the mechanism of Aln-MOF remains to be fully elucidated. Second, this nanoparticle shall be tested in mammal. Further studies are needed to evaluate the drug delivery property of Aln-MOF in the treatment of bone metastases.

Conclusion

This study confirmed that the Aln-MOF prepared by us has good stability, bone targeting and biosafety. After encapsulated with DOX, Aln-MOF$_{DOX}$ was able to rapidly reach higher concentrations at the bone metastases and could effectively kill tumor cells by releasing DOX. Aln-MOF$_{DOX}$ would not damage other normal organs. In summary, Aln-MOF is a new and effective bone targeting nano-delivery carrier, which has a very promising application prospect in the treatment of bone metastasis. We will continue to optimize the characteristics of Aln-MOF and apply it into clinical practice.

Acknowledgments

This study was supported by the Wenzhou Municipal Science and Technology Bureau (Grant number: Y20210400).

Disclosure

The authors report no conflicts of interest in this work.

References

1. Himelstein AL, Foster JC, Khatcheressian JL, et al. Effect of longer-interval vs standard dosing of zoledronic acid on skeletal events in patients with bone metastases: a randomized clinical trial. *JAMA*. 2017;317(1):48–58. doi:10.1001/jama.2016.19425

2. Waning DL, Mohammad KS, Reiken S, et al. Excess TGF-β mediates muscle weakness associated with bone metastases in mice. *Nat Med*. 2015;21(11):1262–1271. doi:10.1038/nm.3961
3. Coleman RE. Clinical features of metastatic bone disease and risk of skeletal morbidity. *Clin Cancer Res*. 2006;12(20):6243s–6249s. doi:10.1158/1078-0432.CCR-06-0931
4. Szade K, Gulati GS, Chan CKF, et al. Where hematopoietic stem cells live: the bone marrow niche. *Antioxid Redox Signal*. 2018;29 (2):191–204. doi:10.1089/ars.2017.7419
5. Gdowski AS, Ranjan A, Vishwanatha JK. Current concepts in bone metastasis, contemporary therapeutic strategies and ongoing clinical trials. *J Exp Clin Cancer Res*. 2017;36(1):108. doi:10.1186/s13046-017-0578-1
6. Weilbaecher KN, Guise TA, McCauley LK. Cancer to bone: a fatal attraction. *Nat Rev Cancer*. 2011;11(6):411–425. doi:10.1038/nrc3055
7. Migliorini F, Maffulli N, Trivellas A, Eschweiler J, Tingart M, Driessen A. Bone metastases: a comprehensive review of the literature. *Mol Biol Rep*. 2020;47(8):6337–6345. doi:10.1007/s11033-020-05684-0
8. Lipton A. Implications of bone metastases and the benefits of bone-targeted therapy. *Semin Oncol*. 2010;37:S15–S29. doi:10.1053/j.seminoncol.2010.10.002
9. Deng X, He G, Liu J, et al. Recent advances in bone-targeted therapies of metastatic prostate cancer. *Cancer Treat Rev*. 2014;40 (6):730–738. doi:10.1016/j.ctrv.2014.04.003
10. Clezardin P, Teti A. Bone metastasis: pathogenesis and therapeutic implications. *Clin Exp Metastasis*. 2007;24(8):599–608. doi:10.1007/s10585-007-9112-8
11. Wippermann B, Mössinger E, Schratt HE, Bastian L, Krettek C. Diagnostik und Therapie von Knochenmetastasen [Diagnosis and therapy of bone metastases]. *Chirurg*. 2001;72(5):638–651. doi:10.1007/PL00002600
12. Doschak MR, Kucharski CM, Wright JE, Zernicke RF, Uludağ H. Improved bone delivery of osteoprotegerin by bisphosphonate conjugation in a rat model of osteoarthritis. *Mol Pharm*. 2009;6:634–640. doi:10.1021/mp8002368
13. Cole LE, Vargo-Gogola T, Roeder RK. Targeted delivery to bone and mineral deposits using bisphosphonate ligands. *Adv Drug Deliv Rev*. 2016;99:12–27. doi:10.1016/j.addr.2015.10.005
14. Crespo L, Sanclimens G, Pons M, Giralt E, Royo M, Albericio F. Peptide and amide bond-containing dendrimers. *Chem Rev*. 2005;105 (5):1663–1681. doi:10.1021/cr030449l
15. Huang X, El-Sayed IH, Qian W, El-Sayed MA. Cancer cell imaging and photothermal therapy in the near-infrared region by using gold nanorods. *J Am Chem Soc*. 2006;128(6):2115–2120. doi:10.1021/ja057254a
16. Chen J, Wang D, Xi J, et al. Immuno gold nanocages with tailored optical properties for targeted photothermal destruction of cancer cells. *Nano Lett*. 2007;7(5):1318–1322. doi:10.1021/nl070345g
17. Della Rocca J, Liu D, Lin W. Nanoscale metal-organic frameworks for biomedical imaging and drug delivery. *Acc Chem Res*. 2011;44 (10):957–968. doi:10.1021/ar200028a
18. Férey G. Hybrid porous solids: past, present, future. *Chem Soc Rev*. 2008;37(1):191–214.
19. Kitagawa S, Kitaura R, Noro S. Functional porous coordination polymers. *Angew Chem Int Ed Engl*. 2004;43(18):2334–2375. doi:10.1002/anie.200300610
20. Duan LN, Dang QQ, Han CY, Zhang XM. An interpenetrated bioactive nonlinear optical MOF containing a coordinated quinolone-like drug and Zn(II) for pH-responsive release. *Dalton Trans*. 2015;44 (4):1800–1804. doi:10.1039/C4DT02672A
21. Rieter WJ, Taylor KM, An H, Lin W, Lin W. Nanoscale metal-organic frameworks as potential multimodal contrast enhancing agents. *J Am Chem Soc*. 2006;128(28):9024–9025. doi:10.1021/ja0627444
22. Di Nunzio MR, Agostoni V, Cohen B, Gref R, Douhal A. A "ship in a bottle" strategy to load a hydrophilic anticancer drug in porous metal organic framework nanoparticles: efficient encapsulation, matrix stabilization, and photodelivery. *J Med Chem*. 2014;57 (2):411–420. doi:10.1021/jm4017202
23. Tan G, Zhong Y, Yang L, Jiang Y, Ren F. A multifunctional MOF-based nanohybrid as injectable implant platform for drug synergistic oral cancer therapy. *Chem Eng J*. 2020;390:124446. doi:10.1016/j.cej.2020.124446
24. Adhikari C, Das A, Chakraborty A. Zeolitic Imidazole Framework (ZIF) nanospheres for easy encapsulation and controlled release of an anticancer drug doxorubicin under different external stimuli: a way toward smart drug delivery system. *Mol Pharm*. 2015;12 (9):3158–3166. doi:10.1021/acs.molpharmaceut.5b00043
25. Ayazi H, Akhavan O, Raoufi M, Varshochian R, Hosseini Motlagh NS, Atyabi F. Graphene aerogel nanoparticles for in-situ loading/pH sensitive releasing anticancer drugs. *Colloids Surf B Biointerfaces*. 2020;186:110712. doi:10.1016/j.colsurfb.2019.110712
26. Wang R, Shou D, Lv O, Kong Y, Deng L, Shen J. pH-Controlled drug delivery with hybrid aerogel of chitosan, carboxymethyl cellulose and graphene oxide as the carrier. *Int J Biol Macromol*. 2017;103:248–253. doi:10.1016/j.ijbiomac.2017.05.064
27. Yang X, Zhai D, Song J, et al. Rhein-PEG-nHA conjugate as a bone targeted drug delivery vehicle for enhanced cancer chemoradiotherapy. *Nanomedicine*. 2020;27:102196. doi:10.1016/j.nano.2020.102196
28. Yin JJ, Pollock CB, Kelly K. Mechanisms of cancer metastasis to the bone. *Cell Res*. 2005;15(1):57–62. doi:10.1038/sj.cr.7290266
29. He F, Matsumoto Y. Basic and clinical associations between bone and cancer. *Immunol Med*. 2020;43(3):103–106. doi:10.1080/25785826.2020.1754084
30. Roodman GD. Mechanisms of bone metastasis. *N Engl J Med*. 2004;350(16):1655–1664. doi:10.1056/NEJMra030831
31. Markovsky E, Koroukhov N, Golomb G. Additive-free albumin nanoparticles of alendronate for attenuating inflammation through monocyte inhibition. *Nanomedicine*. 2007;2(4):545–553. doi:10.2217/17435889.2.4.545
32. McMenemin R, Macdonald G, Moffat L, Bissett D. A Phase II study of caelyx (liposomal doxorubicin) in metastatic carcinoma of the prostate: tolerability and efficacy modification by liposomal encapsulation. *Invest New Drugs*. 2002;20(3):331–337. doi:10.1023/A:1016225024121
33. Minotti G, Menna P, Salvatorelli E, Cairo G, Gianni L. Anthracyclines: molecular advances and pharmacologic developments in antitumor activity and cardiotoxicity. *Pharmacol Rev*. 2004;56(2):185–229. doi:10.1124/pr.56.2.6
34. Susa M, Iyer AK, Ryu K, et al. Doxorubicin loaded polymeric nanoparticulate delivery system to overcome drug resistance in osteosarcoma. *BMC Cancer*. 2009;9:399. doi:10.1186/1471-2407-9-399
35. Fazaeli Y, Akhavan O, Rahighi R, Aboudzadeh MR, Karimi E, Afarideh H. In vivo SPECT imaging of tumors by 198,199Au-labeled graphene oxide nanostructures. *Mater Sci Eng C Mater Biol Appl*. 2014;45:196–204. doi:10.1016/j.msec.2014.09.019
36. Akhavan O, Ghaderi E. Graphene nanomesh promises extremely efficient in vivo photothermal therapy. *Small*. 2013;9 (21):3593–3601. doi:10.1002/smll.201203106
37. Yang K, Zhang S, Zhang G, Sun X, Lee ST, Liu Z. Graphene in mice: ultrahigh in vivo tumor uptake and efficient photothermal therapy. *Nano Lett*. 2010;10(9):3318–3323. doi:10.1021/nl100996u
38. Clarke B. Normal bone anatomy and physiology. *Clin J Am Soc Nephrol*. 2008;3:S131–S139. doi:10.2215/CJN.04151206

39. Carbone EJ, Rajpura K, Allen BN, Cheng E, Ulery BD, Lo KW. Osteotropic nanoscale drug delivery systems based on small molecule bone-targeting moieties. *Nanomedicine*. 2017;13(1):37–47. doi:10.1016/j.nano.2016.08.015
40. Xu XL, Gou WL, Wang AY, et al. Basic research and clinical applications of bisphosphonates in bone disease: what have we learned over the last 40 years? *J Transl Med*. 2013;11:303. doi:10.1186/1479-5876-11-303
41. Nadar RA, Margiotta N, Iafisco M, van den Beucken JJJP, Boerman OC, Leeuwenburgh SCG. Bisphosphonate-functionalized imaging agents, anti-tumor agents and nanocarriers for treatment of bone cancer. *Adv Healthc Mater*. 2017;6(8):1601119. doi:10.1002/adhm.201601119
42. Terpos E, Sezer O, Croucher PI, et al. The use of bisphosphonates in multiple myeloma: recommendations of an expert panel on behalf of the European myeloma network. *Ann Oncol*. 2009;20(8):1303–1317. doi:10.1093/annonc/mdn796
43. Fornari FA, Randolph JK, Yalowich JC, Ritke MK, Gewirtz DA. Interference by doxorubicin with DNA unwinding in MCF-7 breast tumor cells. *Mol Pharmacol*. 1994;45:649–656.
44. Momparler RL, Karon M, Siegel SE, Avila F. Effect of adriamycin on DNA, RNA, and protein synthesis in cell-free systems and intact cells. *Cancer Res*. 1976;36:2891–2895.